# Histotripsy-induced bactericidal activity correlates to size of cavitation cloud in vitro

Pratik A. Ambekar, Yak-Nam Wang, Tatiana Khokhlova, Gilles Thomas, Pavel Rosnitskiy, Kaizer Contreras, Daniel F. Leotta, Adam D. Maxwell, Matthew Bruce, Shelby Pierson, Stephanie Totten, Yashwanth Nanda Kumar, Jeff Thiel, Keith Chan, W. Conrad Liles, Evan P. Dellinger, Adeyinka Adedipe, Wayne Monsky, Thomas J. Matula

***Abstract*— Large abscesses are walled-off collections of pus and bacteria that often do not respond to antibiotic therapy. Standard of care involves percutaneous placement of indwelling catheter(s) for drainage, a long and uncomfortable process with high rehospitalization rates. The long-term goal of this work is to develop therapeutic ultrasound approaches to eradicate bacteria within abscesses as a noninvasive therapeutic alternative. Inertial cavitation induced by short pulses of focused ultrasound (histotripsy) is known to generate lethal mechanical damage in bacteria. Prior studies with *Escherichia coli* (*E. coli*) in suspension demonstrated that bactericidal effects increase with increasing peak negative pressure amplitude, treatment time and duty cycle. The current study investigated correlates of bactericidal activity with histotripsy bubble cloud size produced for these treatment parameters at several ultrasound frequencies. Histotripsy was applied to *E. coli* suspensions in 10-mL sample vials at 810 kHz, 1.2 MHz, or 3.25 MHz for 40 minutes. The resulting cavitation activity in the sample vials was separately observed with high-speed photography. The bubble cloud area was quantified from those images. A linear relationship was observed between log kill and cavitation cloud size ($R^2$ = 0.96), regardless of the acoustic parameters (specifically frequency, pulse duration and pressure amplitude) used to produce the cloud. These findings suggest a role for *in-situ* treatment monitoring using B-mode imaging.**

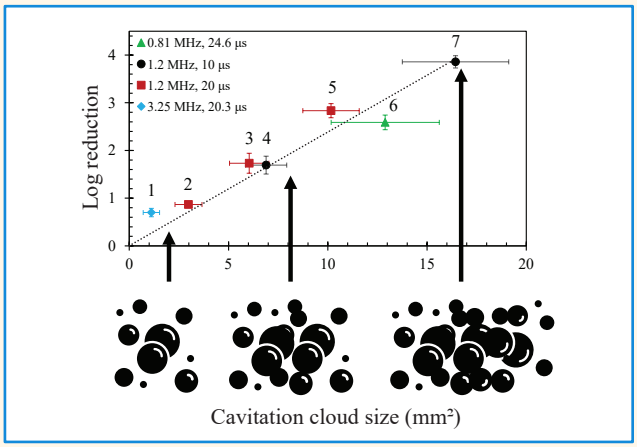


***Index Terms*—Abscess, Bacterial inactivation, Cavitation, High intensity focused ultrasound (HIFU), Histotripsy, Therapeutic ultrasound.**

## I. Introduction

ULTRASOUND-mediated microbial inactivation is contingent upon a myriad of non-acoustic determinants, such as the organism's taxonomic classification, pH level, and temperature, alongside the acoustic determinants: ultrasound frequency, peak pressure amplitude, pulse length, pulse repetition frequency (PRF),

This work was supported in part by NIH grants R01AR080120, R01EB023910, R01GM122859 and R01EB031788.x

P. A. Ambekar, YN Wang, J. Thomas, K. Contreras, D. F. Leotta, M. Bruce, S. Totten, Y. N. Kumar, J. Thiel, and T. J. Matula are with the Center for Industrial and Medical Ultrasound, Applied Physics Laboratory, University of Washington, Seattle, USA (email: matula@uw.edu).

T. Khokhlova and P. Rosnitskiy are with the Dept. of Gastroenterology, University of Washington, Seattle, USA.

A. D. Maxwell is currently at the Dept. of Biomedical Engineering and Mechanics, Virginia Tech, Blacksburg, Virginia, USA.

S. Pierson is with California polytechnic state university, San Luis Obispo, USA.

K. Chan is with Vantage Radiology and Diagnostic Services, Renton WA, USA.

W. C. Liles is with Dept. of Medicine, University of Washington, Seattle, USA.

E. P. Dellinger is at the Dept. of Surgery, University of Washington, Seattle, USA.

A. Adedipe is with the Dept. of Emergency Medicine, University of Washington, Seattle, USA

W. Monsky is at the Dept. of Radiology, University of Washington, Seattle, USA.

***Highlights***

- **The degree of bacterial inactivation by histotripsy depends upon several acoustic variables such as pressure, frequency, duty cycle, and treatment time.**
- **Over a range of frequencies, powers, and pulse lengths, the cavitation cloud axial cross-sectional area correlated with bacterial inactivation.**
- **The *in-situ* efficacy of abscess treatment with histotripsy may be quantifiable by measuring the cloud area using B-mode images from a standard diagnostic ultrasound imaging system.**

duty cycle, treatment duration, characteristics of the suspending medium (e.g., volume, composition, and viscosity), and absorption-induced heating. Previous studies that used immersion transducers (horns or unfocused disks) demonstrated that *Escherichia coli* (*E. coli*) bactericidal activity exhibits a pronounced dependence on ultrasound frequency, decreasing as frequency increases [1, 2]. Studies that used violent inertial cavitation activity induced by short high-amplitude focused ultrasound (FUS) pulses – histotripsy – found that increasing peak acoustic pressures, treatment duration, and duty cycle enhance bactericidal rates [3]. Conversely, pulse duration does not affect bacterial inactivation if the duty cycle remains constant. The mechanism underpinning non-thermal germicidal action of FUS predominantly points to direct mechanical effects associated with shear forces during the collapse of cavitation bubbles [4, 5].

The implementation of histotripsy-based bactericidal activity implies the formation of dense cavitation bubble clouds through the delivery of high-amplitude short (1 to 50 cycles) pulses at low pulse repetition frequency (PRF) [6, 7]. Histotripsy has been successfully applied to removal of bacterial biofilms [8-10] and inactivation of bacteria in suspensions *in vitro* [3, 9, 11], and also *in vivo* in a porcine abscess model [12]. However, due to the extensive parameter space outlined above, selecting the most pertinent acoustic variables for treatment poses a challenge. Simplifying predictions of inactivation rates by identifying a singular predictive parameter would be important for clinical implementation.

Of particular note, the pressure amplitude threshold requisite for *E. coli* inactivation aligned with the threshold for consistent cavitation cloud formation pulse to pulse [3]. The inactivation of *E. coli* over time followed pseudo-first order kinetics when plotted as a log-linear graph (similar pseudo-first order kinetics were also recently reported for Pseudomonas Aeruginosa in suspension [11]. However, the pseudo-rate constants (slope of kill vs. time) depended greatly on the acoustic variables, changing by up to a factor of 6 over the parameter space studied. The clinical need to identify an appropriate acoustic parameter space and to predict the expected kill is thus a formidable challenge. Moreover, the impracticality of sample removal for characterization or treatment monitoring further compounds the clinical challenge of prognosticating outcomes based on a specific parameter.

The characteristics of the bubble cloud formed by the histotripsy pulses – its overall size, density, distribution, the sizes of the bubbles within it, and collapse time – are known to be dependent on the acoustic exposure parameters and to determine the outcomes in soft tissue ablation [13, 14]. The two observations that 1) being above the consistent cavitation threshold (having a cavitation cloud each pulse) is required for bactericidal activity, and 2) the cloud characteristics depend on the acoustic parameters, suggest that the characteristics of the cavitation cloud itself may be correlative indicators of bactericidal activity. If this hypothesis held, in a clinical implementation it would be possible to ensure consistent cloud formation and measure its characteristics via a combination of passive cavitation detection (PCD) and coaxial synchronized ultrasound imaging. In this work we test the hypothesis that bactericidal effects of histotripsy on liquid bacterial suspensions can universally be attributed to the size of the bubble cloud, regardless of the specific acoustic parameter sets that had led to the formation of that bubble cloud.

The most comprehensive way of characterizing histotripsy cavitation clouds *in vitro* is high-speed optical imaging [14]. It is with this technique that we investigate the potential for a single correlative factor – the cavitation cloud size – to predict bactericidal activity over a range of acoustic parameters, including frequency, pressure amplitude, and pulse length.

## II. Methods

### A. Culture and preparation

*Escherichia coli (E. coli)* FDA strain Seattle 1946 was purchased from the American Type Culture Collection (ATCC, Manassas, VA, USA). The bacteria were maintained as a streak culture in a 3% tryptic soy broth (TSP) medium with 2% agar. Details for the preparation and use of the bacteria are described elsewhere [15]. Bacterial growth was

monitored by periodically measuring the optical density at 600 nm (OD600). The culture was used after reaching the stationary phase, as predetermined from previous growth characteristics studies.

### B. Histotripsy exposure apparatus

This study utilized two histotripsy transducers operated across three frequencies (0.81 MHz, 1.20 MHz, and 3.25 MHz). One transducer (H-161, Sonic Concepts, Bothell, WA) was electrically matched and operated at either 0.81 MHz or 1.20 MHz. At the 0.81 MHz frequency the transducer was driven by a function generator (33250A, Agilent, Santa Clara, CA) and amplifier (AG 1012, T&C Power Conversion, Inc., Rochester, NY), while at 1.2 MHz it was driven by a dedicated controller (TPO-401, Sonic Concepts). A custom-made transducer fabricated in-house [16], operating at 3.25 MHz, was driven by the same function generator and amplifier. The transducer specifications and pulse parameters for these studies are listed in Table I.

Two custom experimental apparatuses were used for the studies, as shown in Fig. 1. At 0.81 or 1.20 MHz (Fig. 1a), the H-161 transducer was mounted to the bottom of a cylindrical tube (15.2 cm diameter, 0.8 cm wall thickness, and 18 cm in height) filled with degassed water for coupling between the transducer and the sample vial. At 3.25 MHz, (Fig. 1b) the transducer was positioned in a large, degassed water bath (not shown in the figure).

For either apparatus, the sample vial contained 10 ml of bacteria culture (~$10^8$ cfu/ml). The bottom of each vial (2.5 cm outer diameter, 0.3 cm wall thickness, and 4.6 cm height) was replaced with an acoustically transparent polyethylene membrane held with an O-ring nestled in an annulus machined into the bottom outer surface. The proximal wall of the membrane was wiped with a gauze sponge to eliminate pre-existing bubbles that could interfere with the ultrasound pulse. The water was kept degassed to <20% of saturation. Alignment was verified by inducing cavitation within the vial and carefully positioning it so that cavitation was induced 15 mm above the bottom membrane.

Table I. Transducer specifications and pulse protocol for bubble cloud imaging experiments.

| Transducer | Sonic Concepts H-161 | Sonic Concepts H-161 | Custom |
|---|---|---|---|
| Frequency | 0.81 MHz | 1.20 MHz | 3.25 MHz |
| Central opening diameter | 47 mm | 47 mm | None |
| Aperture | 134.9 mm | 134.9 mm | 41 mm |
| Focal distance | 124.5 mm | 124.5 mm | 45 mm |
| F-number | 0.92 | 0.92 | 1.09 |
| Pulse duration | 24.6 µs | 10 µs or 20 µs | 20.3 µs |
| Pulse repetition frequency | 406 Hz | 1000 Hz or 500 Hz | 492 Hz |
| Number of pulses | 975,609 | 1,200,000 | 1,182,266 |
| Acoustic power(s) | 926 W | 248 W to 1090 W | 87 W |
| Camera exposure time | 25 µs | 13 µs or 25 µs | 25 µs |

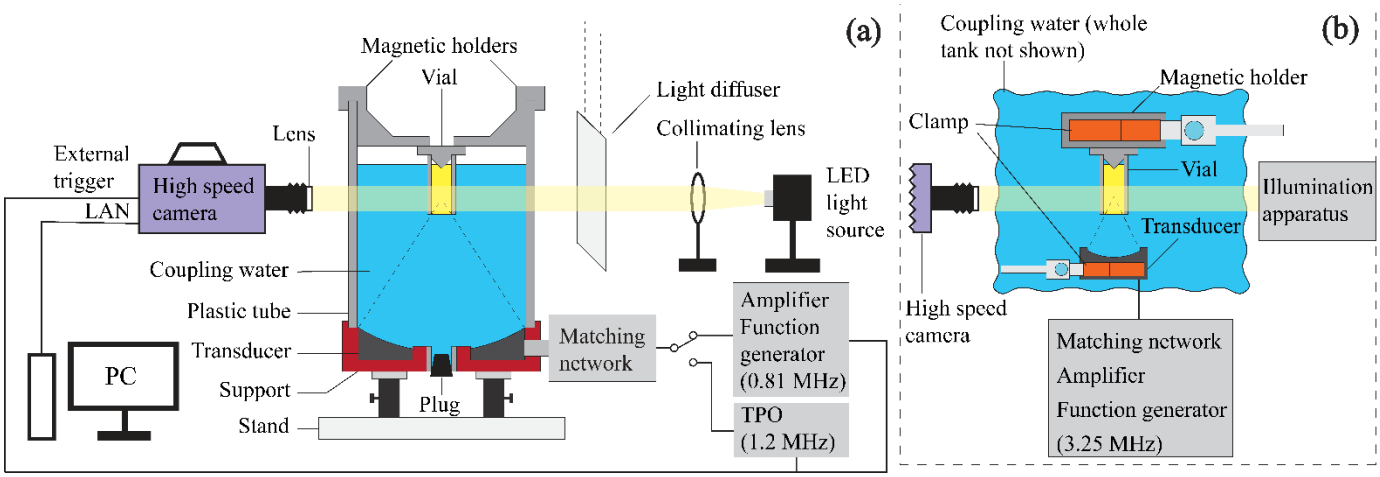


Figure 1. Experimental setups for cavitation cloud imaging at three different frequencies. (a) Studies at 0.81 and 1.2 MHz were conducted with a Sonic Concepts transducer (model H-161) mounted to a cylindrical water bath degassed to < 20% saturation. The sample vial was held with magnets that kept the vial aligned with the transducer. (b) Studies at 3.25 MHz were performed with a custom-built transducer immersed in a large degassed (< 20%) water bath. Alignment of the transducer and sample vial were performed manually, as described in the text. For either setup, cavitation was generated at the focus, 15 mm above the vial's bottom, approximately at the center of the vial. The same LED light source back-illuminated the cavitation cloud. Additional details are described in the text.

Calibration of the transducer focal pressure levels at the full range of system driving voltages was performed in degassed water with a fiber-optic probe hydrophone (FOPH 2000; RP Acoustics, Lautenbach, Germany; 100 µm active diameter, 100 MHz bandwidth). The sample vial was removed for characterization. At 3.25 MHz measurements could not be performed at the highest output levels due to the occurrence of cavitation at the fiber tip. Hence, to obtain focal pressure waveforms at those levels, axially symmetric nonlinear field simulations were performed using a freely available open-source HIFU-beam software (https://limu.msu.ru/) based on solving the one-way propagation radially symmetric Westervelt equation [17]. We assumed that the input voltage to the transducer was proportional to the characteristic pressure at the transducer surface. The focal pressures from the simulations

were matched to the experimentally calibrated points and extrapolated to higher voltages. Fig. 2c shows the simulated waveform at 3.25 MHz. HIFU-beam simulations were also conducted at 0.81 MHz and 1.20 MHz and the simulated waveforms were aligned with those observed experimentally, as illustrated in Fig. 2a and 2b. All waveforms in Fig. 2 correspond to the output level at which the consistent cavitation threshold was achieved. Total acoustic power was noted at each simulation waveform corresponding to the experimental waveform at all frequencies.

The consistent cavitation threshold was identified for each frequency in the bacteria culture. All experiments were conducted above these thresholds - a prerequisite for bacterial inactivation as demonstrated in our previous work [3].

### C. Bubble cloud visualization experiments

A high-speed camera (Photron Fastrax APS-RX, Photron, San Diego, California, USA) was utilized to visualize bubble clouds. Because *E. coli* cultures used in the inactivation studies were too turbid for obtaining clear images of the bubble clouds, transparent growth medium (3% TSB) was used instead. For this reason, the bubble cloud visualization experiments were conducted separately from the *E. coli* inactivation treatments. The growth medium was preheated in the incubator at 37°C for the same duration as the *E. coli* cultures to replicate their pre-treatment conditions.

As shown in Fig. 1, the high-speed camera was focused on the transducer's focal region using an 80 to 200 mm zoom lens to capture grayscale images of the bubble clouds. Proper lateral alignment was ensured by adjusting the camera until the diametrically opposite sides of the sample vial looked equally sharp. The vial was backlit by an LED and passed through a collimator lens and diffuser to provide uniform background light intensity. The camera shutter was triggered by the electronics driving the transducer, ensuring that an acquisition occurred at each histotripsy pulse. The acquisition was delayed by the time of flight from the transducer to the focus, and the frame rate corresponded to the pulse repetition frequency of the transducer. The shutter speed was set to be slightly longer than the pulse duration (Table I) across all frequencies, allowing for the recording of the average grayscale intensity throughout the entire pulse duration. At each frequency, images were captured at a resolution of 1024*x*1024 pixels, with 1000 frames recorded per acoustic power setting. A few frames were recorded before starting the transducer and were later used for background noise subtraction. The pixel-to-mm ratio was determined in Image-J by taking the reference of known vial diameter and was 43 to 48 microns/pixel.

Figure 3a shows a representative grayscale image of a bubble cloud. To calculate the area of the cloud, the image was processed in MATLAB (Natick, MA) as follows. First, the background image noted above was subtracted from all frames. Bubble clouds were identified using binary gray level thresholding segmentation, as a group of dark pixels (Fig. 3b). The exterior boundary of each bubble cloud was traced using the Moore-Neighbor algorithm [18], and the cross-sectional area was determined by counting the number of black pixels within these boundaries. The pixel area was converted to square

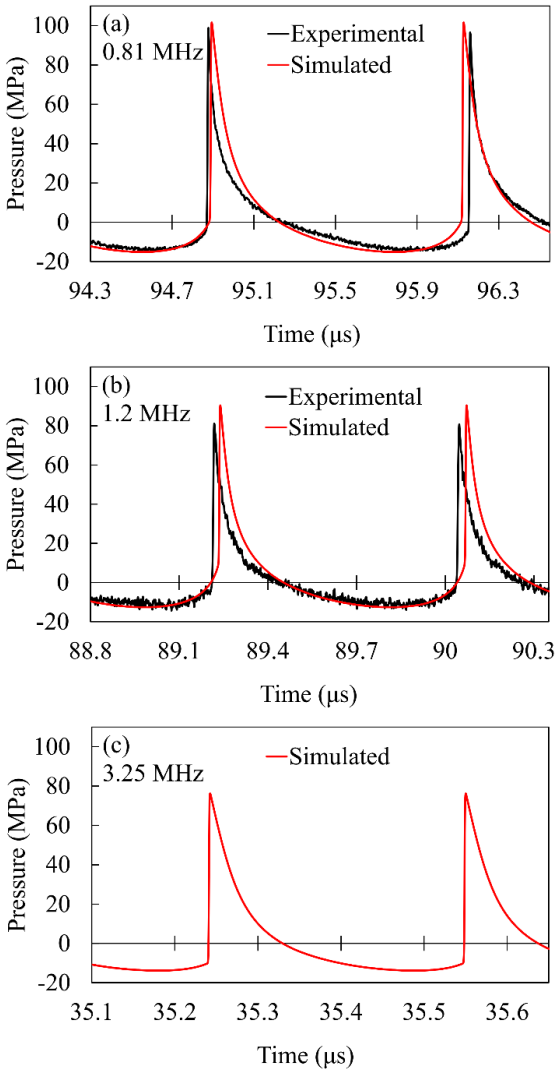


Figure 2. Focal pressure waveforms at the three frequencies from hydrophone measurements and numerical simulations. The waveforms correspond to the output acoustic power just above consistent cavitation thresholds as follows: a) Frequency = 0.81 MHz, Acoustic power = 926 W b) Frequency = 1.20 MHz, Acoustic power = 268 W c) Frequency = 3.25 MHz, Acoustic power = 87 W. At 3.25 MHz hydrophone measurements could not be performed due to the cavitation occurring at the hydrophone tip.

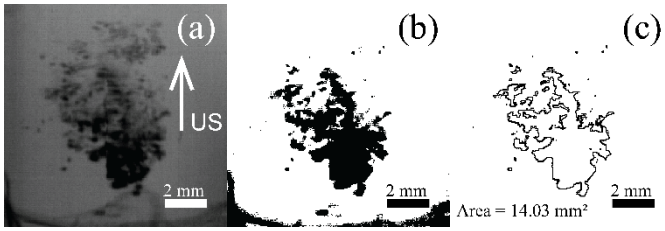


Figure 3. Image processing of grayscale images to obtain bubble cloud area. a) Representative grayscale image at 0.81 MHz, 24.6 $\mu$s pulse duration, 926 W acoustic power. The arrow is in the direction of the histotripsy pulse. b) Conversion to binary image based on a binary threshold. c) The outline of the bubble clouds (black) in the binary images was highlighted and area was calculated based on the number of pixels. Note that the dark region at the bottom of Fig. 3b which corresponds to the vial membrane is not included in the area calculation.

millimeters (Fig. 3c). The bubble cloud area was averaged and the standard deviation was calculated.

### D. Exposure protocol

The treatment parameters used with each apparatus are shown in Table II. All treatments were performed for 40 minutes at 1% duty cycle making the total on-time 24 seconds for each treatment. Four pulse protocols were applied: 20.3 µs pulse duration (66 cycles) at 3.25 MHz; 10 µs or 20 µs pulse duration (12 or 24 cycles) at 1.20 MHz; and 24.6 µs pulse duration (20 cycles) at 0.81 MHz. At frequencies 0.81 MHz and 3.25 MHz, only a single acoustic power setting was sufficient to exceed the consistent cavitation threshold, whereas for 1.20 MHz, multiple acoustic power settings exceeded the cavitation threshold. Overall, inactivation experiments were conducted at seven distinct pulse protocols and each treatment was repeated four times.

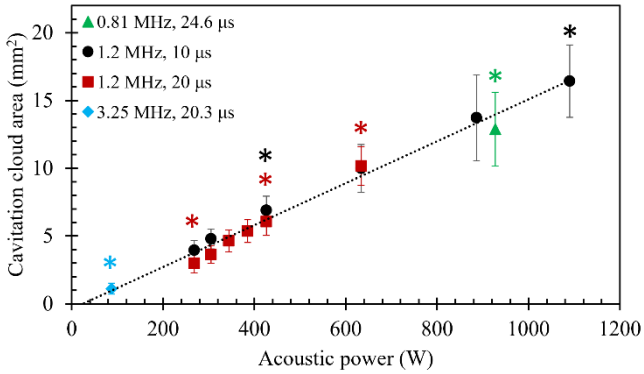


Figure 4. Bubble cloud area dependence on peak acoustic power for the three frequencies and two pulse durations. Error bars correspond to standard deviation of the bubble cloud area across histotripsy pulses. The dependence is close to linear ($R^2$=0.98), regardless of the frequency and pulse duration. Points marked with a star indicate the protocols used for inactivation experiments.

### E. Viability assessment

Samples withdrawn from the treated cell suspensions were subjected to serial dilutions with EPA dilution water (2 mM MgCl2, 0.6 mM $KH_2PO_4$, pH 7.1) as a standard diluent for *E. coli* using aliquots no smaller than 25 µL, as described previously [15]. The diluted samples (1 ml) were deposited onto compact Dry EC100 assay plates (Hardy Diagnostics, Santa Maria, CA, USA) on which *E. coli* produces a blue colony while non-*E. coli* coliforms produce red colonies. Colonies were manually counted after incubation at 37°C for ~18 hr., when the colonies were visible macroscopically. Control samples were taken before and after each treatment and log10 of the ratio of the pre-treatment count to the post-treatment count was calculated. Each treatment was repeated at least four times.

Table II. Treatment parameters for E. coli inactivation experiments.

| Data point | Frequency (MHz) | Pulse (µs) | Cycles | Acoustic Power (W) | Cavitation cloud area ($mm^2$) |
|---|---|---|---|---|---|
| 1 | 3.25 | 20.3 | 66 | 87 | 1.11 |
| 2 | 1.2 | 20 | 24 | 268 | 2.98 |
| 3 | 1.2 | 20 | 24 | 425 | 6.06 |
| 4 | 1.2 | 10 | 12 | 425 | 6.89 |
| 5 | 1.2 | 20 | 24 | 633 | 10.21 |
| 6 | 0.81 | 24.6 | 20 | 926 | 12.89 |
| 7 | 1.2 | 10 | 12 | 1090 | 16.71 |

### F. Statistical analysis

We investigated the relationship between *E. coli* log kill and the bubble cloud area using linear regression. For the regression analysis, each data point was considered independently rather than averaging the log kill corresponding to the same treatment parameters. As a result, the sample size for regression was 28. The coefficient of determination and coefficient of correlation were calculated in MATLAB.

## III. Results

### A. Bubble cloud images

Fig. 4 shows representative bubble cloud grayscale images at the three frequencies just above the consistent cavitation threshold; ultrasound is incident from the bottom of the images. In each image, a black region is visible pre-focally, corresponding to a dense bubble cloud, which transitions to lighter shades of gray post-focally, indicating smaller and/or sparser bubbles. As expected, bubble cloud size decreases with an increase in frequency. The area of the bubble clouds in the frames are 14.03 $mm^2$, 3.54 $mm^2$, 1.53 $mm^2$ for 0.81 MHz, 1.20 MHz, and 3.25 MHz respectively. Additionally, the shape of the bubble cloud at 0.81 MHz exhibits a more circular configuration, while at higher frequencies of 1.20 MHz and 3.25 MHz, the clouds assume an increasingly elliptical shape.

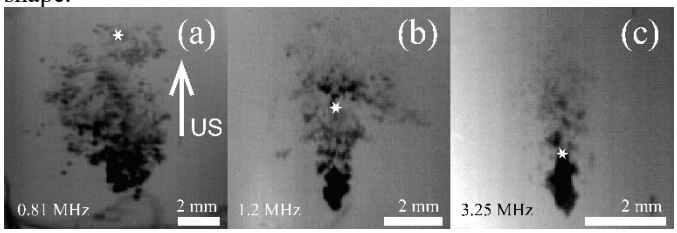


Figure 5. Bubble cloud grayscale images in the growth medium (3% Tryptic Soy Broth) at the three frequencies just above the consistent cavitation threshold. The white star indicates geometric focus. a) Frequency = 0.81 MHz, Acoustic power = 926 W b) Frequency = 1.20 MHz, pulse duration 20 $\mu$s, Acoustic power = 268 W c) Frequency = 3.25 MHz, Acoustic power = 87 W. A decrease in dimensions with increasing frequency is observed.

Figure 5 illustrates representative bubble clouds visualized at 1.20 MHz, 20 µs pulse length, at increasing acoustic powers ranging from 268 W to 1090 W. The white star in each image indicates the geometric focus. With increasing acoustic power, we observe an increase in the bubble cloud length and width. The proximal border of the cloud moves towards the transducer as the acoustic power increases, while there is minimal shift of the distal border. At higher acoustic powers the bubbles in the post-focal regions were entrapped in vortical flow patterns (Fig. 5 d-i). Those flow patterns were previously reported for

histotripsy clouds within confined spaces in the context of intravascular thrombolysis [19].

For all experiments, the exposure time was slightly longer than the pulse duration, which captures the cloud near its maximum size. That is, bubbles scatter more light when they are large and also spend more time near their maximum size. Thus, when averaged over the pulse duration, the images correspond to bubbles near their maximum size. The variation in intensity across the cloud is most probably due to differences in bubble density and maximum size. Lighter regions above the darker regions may represent residual bubbles from previous pulses entrained in the vortical streaming pattern. Binary thresholding focused on resolving the shape of the dark region of the cloud. Therefore, some bubble regions with grayscale values above the binary threshold, particularly in the upper region of the cloud, were not included in the analysis. An example is seen in Fig. (3a,b).

### B. Bubble cloud area dependence on acoustic power

Fig. 6 shows the measured size of the bubble cloud area (in $mm^2$) as a function of acoustic power at the different frequencies and pulse lengths; points marked with a star represent protocols used for both cavitation imaging and bacterial inactivation experiments. Error bars represent standard deviation of bubble cloud area across histotripsy pulses. At 1.20 MHz, the cloud sizes for the two pulse lengths were similar within the measurement uncertainty. As mentioned previously, at frequencies 0.81 MHz and 3.25 MHz, only a single acoustic power level was used.

Looking at Fig. 6 and the area values from Table II, the bubble cloud area increases linearly ($R^2$=0.98) with acoustic power over a range of frequencies and pulse lengths. That is, over the parameters that were studied, the bubble cloud area dependence on the acoustic power is linear regardless of the other parameters. The variability in bubble cloud size from pulse to pulse also increases with acoustic power, as evidenced by larger standard deviation bars.

### C. E. coli inactivation dependence on cloud area

Inactivation treatments were conducted at seven distinct pulse protocols which are listed in Table II and also marked with stars in Figure 6. A strong linear relationship ($R^2$ = 0.98, R = 0.99, and $p < 0.0001$) between *E. coli* log inactivation and the bubble cloud area was observed (Fig. 7). The highest log kill was 3.85 and was achieved at the frequency of 1.20 MHz, pulse duration of 10 μs and an acoustic power of 1090 W.

While individual data points were used to fit the regression line at each treatment level, the plot displays these points as average and standard deviation for each treatment. The regression equation is y = 0.23*x. The slope of 0.23 suggests that each 4.3 $mm^2$ increase in bubble cloud area leads to an additional log kill of 1.

## IV. Discussion

The major findings of this study point to the cavitation cloud size as a *single* determinant for predicting *E. coli* inactivation because of the linear correlation between cloud area and inactivation (Fig. 7). Moreover, the linear correlation exists irrespective of the parameters used (Table II: three different frequencies, four pulse lengths, five power levels), thus supporting the original hypothesis. It is envisioned that these important findings might lead to an ultrasound-based method to monitor treatments *in situ* independent of the treatment device and pulsing parameters.

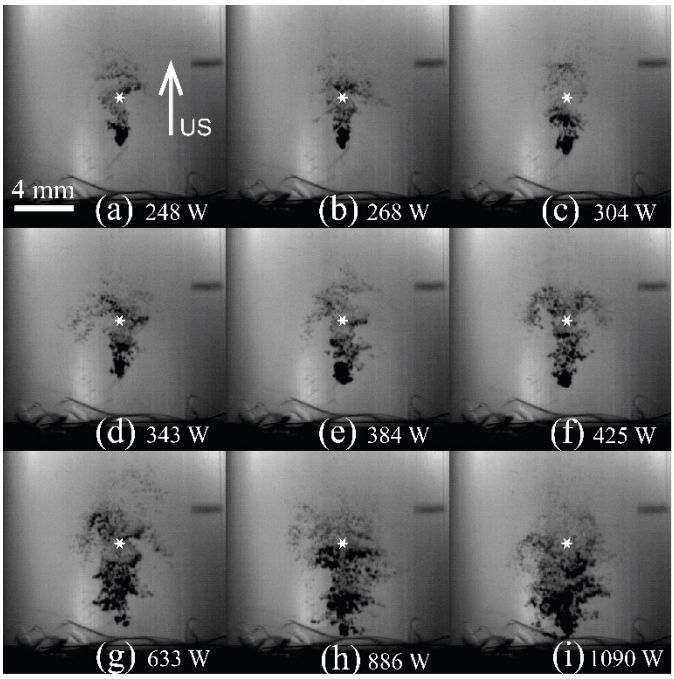


Figure 6. Bubble cloud grayscale images in the growth medium (3% Tryptic Soy Broth) at 1.20 MHz, 20 μs with increasing acoustic powers. Geometric focus is marked with a white star for reference. With increasing power, we observe that bubble cloud size increases and the cloud shifts pre-focally.

The opacity of *E. coli* in suspension precluded simultaneous measurements of the cloud dimensions and *E. coli* inactivation. Instead, separate experiments using identical parameters were performed, one to measure cavitation cloud dimensions in optically transparent TSB without bacteria, and the other to evaluate *E. coli* inactivation in suspension. The bubble cloud area was measured via high-speed photography under different pulse protocols with varying frequency, pulse duration, and acoustic power. Then a subset of those protocols was used to inactivate *E. coli* suspensions and evaluate the kill by colony counting.

In this work, we chose peak acoustic power as the independent variable in experiments measuring the cavitation cloud size instead of peak negative pressure amplitude ($P^-$) commonly used in cavitation-based studies. This is due to utilization of the shock-scattering histotripsy regime. In this regime, reflection, inversion and scattering of the compressive shock from a single bubble leads to the formation of bubble clouds. Peak positive pressure (P+) and high-amplitude shock formation are thus requirements for the formation of bubble clouds, and $P^-$ alone does not fully describe the corresponding output level [6].

One of the major findings of this work is that the bubble cloud area depended linearly on the acoustic power for all frequencies and was independent of pulse length (Fig. 6). The pulse length independence could be attributed to the relatively long – 10 and 20 us – pulse durations. The axial size of the bubble cloud is known to grow with pulse duration, but saturate beyond a certain value, and the lateral size is independent of it [6].

For any set frequency, the linear dependence of the bubble cloud area on acoustic power can be explained as follows. The shape and dimensions of the bubble cloud are determined by those of the area within which the high-amplitude shocks are formed. At the output levels beyond shock formation regime, P+ grows nearly linearly with pressure at the transducer surface $P_0$, and so do both lateral and axial dimensions of the area around the focus where shocks are formed [17, 20]. Because the area is proportional to the product of the two axial dimensions, and thus to $P_0^2$, it is, in turn, linearly proportional to acoustic power.

Interestingly, the bubble cloud areas corresponding to consistent cavitation threshold at three different frequencies were close to the same linear relationship on acoustic power. This similarity can be explained as follows. The acoustic power that is necessary to achieve a certain focal pressure level in the linear regime has an inverse quadratic dependence on frequency for spherically-focused transducers [21]. In the nonlinear regime, the focal pressure levels $P^+$ and $P^-$ at which the shocks form are known to be similar, regardless of the frequency, provided similar F-numbers of the transducers – in our case 0.92 and 1.1. The dependence of acoustic power at which the shocks (and hence the bubble clouds) form on frequency is also close to inverse quadratic [20]. Therefore, the acoustic power at which the shocks (and hence the bubble clouds) form can be expected to also follow the inverse quadratic dependence on frequency. The axial and lateral dimensions of the bubble cloud are determined by those of the transducer's focal area, which are both inversely proportional to the ultrasound frequency [21], thus its area is inversely proportional to the square thereof. Since both the acoustic power and the 2D axial cross-sectional area of the bubble cloud at the threshold of its formation depend on frequency in the same way (inverse quadratic), it was reasonable to expect close to linear proportionality between them for different frequencies. This expectation was experimentally confirmed (Fig. 6). However, it is important to note that this linear proportionality should not be expected to be universally applicable and is limited to the F-numbers and aperture-to-wavelength ratios considered here.

The effects of acoustic parameters on shock-scattering histotripsy bubble clouds have been studied via high-speed photography in phantoms and water [6, 10, 22]. In this work, the clouds were produced in a confined volume (10ml) of TSB solution with dissolved gas concentration relevant to cultured bacterial suspensions. Higher gas concentrations affect cavitation bubble and cloud dynamics, and the confined volume (relevant to treating abscesses) affects the structure of vortical streaming patterns [19]. Furthermore, a range of acoustic parameters previously shown to result in clinically relevant inactivation [3, 12] and applicable to abscesses of variable sizes

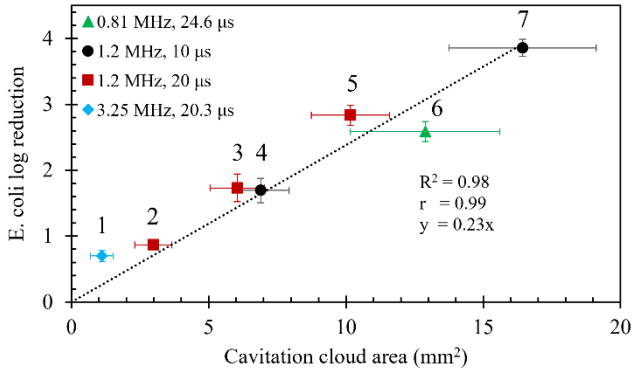


Figure 7. *E. coli* log reduction dependence on bubble cloud area. Seven pulse protocols marked with a star in Fig.6 and also listed in Table II were applied to 10 mL *E. coli* suspensions for 40 minutes. A strong linear dependence of log reduction on the bubble cloud area was observed (R = 0.96, p < 0.0001, n=4). Vertical error bars correspond to standard deviation of log kill, while horizontal error bars correspond to the standard deviation of the bubble cloud area from Fig.6.

located at varying depths had to be considered. This necessitated the optical observation of the bubble clouds performed here. In prior work histotripsy cavitation activity in bacterial suspension was characterized via coaxial ultrasound B-mode imaging and passive cavitation detection (PCD) that quantified broadband noise emissions from inertially collapsing bubbles [3]. However, no predictive relationship between PCD-based metrics and log kill was identified in those studies, which was hypothetically attributed to shielding of the emissions by the proximal layers of the bubbles in the cloud. In light of the high-speed photography observations of the bubble clouds here (Fig. 5) a different explanation appears more plausible: bacterial kill depends not only on the presence of inertial bubble collapses, but also on the number of those bubbles, i.e. the bubble cloud dimensions, which cannot be captured by single-channel PCD, as it is not spatially resolved.

Seven disparate histotripsy pulse protocols consisting of three different frequencies, different pulse durations and a range of acoustic powers were used to create the bubble clouds to induce *E. coli* inactivation. Yet across all those parameter combinations the *E. coli* inactivation correlated well with the bubble cloud area. This suggests that bubble cloud area can be used as a predictive indicator of bacteria inactivation. In clinical context, bubble clouds can be readily visualized by coaxial B-mode ultrasound imaging [3], and their dimensions can be measured to predict the treatment time necessary for a specific log kill.

The study is not without limitations. First, a fixed volume of bacterial suspension was used in the inactivation studies; due to the presence of high-speed vortical flow it may be expected that the entire volume of the suspension is circulated through the area with active bubble cloud. If the volume is thus constrained, it may then be reasonably predicted that the bubble cloud of the same size will produce a lower log kill in a larger liquid volume. For larger volumes, the size of the bubble cloud alone may not be predictive of the log kill; rather, the ratio of that area to the liquid volume should be a better determinant for predicting bactericidal activity. This dependence will be clarified in future studies.

The second limitation is that optical imaging of the bubble cloud size and inactivation studies had to be performed in separate experimental sets due to the high turbidity of bacterial suspensions. However, the cavitation thresholds in TSB and bacterial suspension (quantified for all frequencies) were similar, as was the gas content. Thus, the differences in the bubble cloud size should not be significant. Further, due to the specific configurations of the experimental setup – very large focal distance for the lower frequency transducer and the absence of the opening for the imaging probe in the high frequency transducer – coaxial B-mode US imaging could not be performed with sufficient spatial resolution to compare the bubble cloud size measurements with optical imaging. This will be performed in future studies, with a clinically relevant histotripsy transducer and a high-quality/large-aperture ultrasound imaging probe.

## V. Conclusion

Shock-scattering histotripsy was used to treat a constrained volume of *E. coli* in suspension. Separately, the induced cavitation cloud was optically imaged in the same volume, without bacteria. Acoustic parameters included three different frequencies, as well as several pulse lengths and power levels. It was found that the size of the cavitation cloud depended linearly on the acoustic power level for all frequencies and was independent of the pulse length. Similarly, *E. coli* inactivation was linearly correlated to the size of the cavitation cloud, irrespective of the other parameters. This has implications for clinical abscess treatment, as it may be possible to use ultrasound imaging to quantify cloud size and thus predict bactericidal rates.

## References


1. Hashimoto, Y., et al., *Inactivation of Escherichia coli, Saccharomyces cerevisiae and Bacillus subtilis by ultrasonic cavitation.* Acoustical Science and Technology, 2020. **41**(6): p. 877-884.
2. Hua, I. and J.E. Thompson, *Inactivation of Escherichia coli by sonication at discrete ultrasonic frequencies.* Water Research, 2000. **34**(15): p. 3888-3893.
3. Ambekar, P.A., et al., *Comparative Study of Histotripsy Pulse Parameters Used to Inactivate Escherichia coli in Suspension.* Ultrasound Med Biol, 2023. **49**(12): p. 2451-2458.
4. Gao, S., et al., *Inactivation of microorganisms by low-frequency high-power ultrasound: 2. A simple model for the inactivation mechanism.* Ultrasonics sonochemistry, 2014. **21**(1): p. 454-60. PMID: 23845410.
5. Brayman, A.A., et al., *Inactivation of Planktonic Escherichia coli by Focused 1-MHz Ultrasound Pulses with Shocks: Efficacy and Kinetics Upon Volume Scale-Up.* Ultrasound Med Biol, 2018. **44**(9): p. 1996-2008.
6. Maxwell, A.D., et al., *Cavitation clouds created by shock scattering from bubbles during histotripsy.* J Acoust Soc Am, 2011. **130**(4): p. 1888-98.
7. Lin, K.W., et al., *Histotripsy beyond the intrinsic cavitation threshold using very short ultrasound pulses: microtripsy.* IEEE Trans Ultrason Ferroelectr Freq Control, 2014. **61**(2): p. 251-65.
8. Bigelow, T.A., et al., *The destruction of Escherichia coli biofilms using high-intensity focused ultrasound.* Ultrasound Med Biol, 2009. **35**(6): p. 1026-31.
9. Bigelow, T.A., et al., *Histotripsy Treatment of S. Aureus Biofilms on Surgical Mesh Samples Under Varying Pulse Durations.* IEEE Trans Ultrason Ferroelectr Freq Control, 2017. **64**(10): p. 1420-1428.
10. Childers, C., et al., *Focused Ultrasound Biofilm Ablation: Investigation of Histotripsy for the Treatment of Catheter-Associated Urinary Tract Infections (CAUTIs).* IEEE Trans Ultrason Ferroelectr Freq Control, 2021. **68**(9): p. 2965-2980.
11. Morse, R., et al., *Catheter-Based Medical Device Biofilm Ablation Using Histotripsy: A Parameter Study.* Ultrasound Med Biol, 2023. **49**(9): p. 2152-2159.
12. Matula, T.J., et al., *Treating Porcine Abscesses with Histotripsy: A Pilot Study.* Ultrasound Med Biol, 2021. **47**(3): p. 603-619.
13. Vlaisavljevich, E., et al., *Histotripsy-induced cavitation cloud initiation thresholds in tissues of different mechanical properties.* IEEE Trans Ultrason Ferroelectr Freq Control, 2014. **61**(2): p. 341-52.
14. Nanda Kumar, Y., et al., *Development of Tough Hydrogel Phantoms to Mimic Fibrous Tissue for Focused Ultrasound Therapies.* Ultrasound Med Biol, 2022. **48**(9): p. 1762-1777.
15. Brayman, A.A., et al., *Inactivation of Planktonic Escherichia coli by Focused 2-MHz Ultrasound.* Ultrasound Med Biol, 2017. **43**(7): p. 1476-1485.
16. Canney, M.S., et al., *Acoustic characterization of high intensity focused ultrasound fields: a combined measurement and modeling approach.* J Acoust Soc Am, 2008. **124**(4): p. 2406-20.
17. Yuldashev, P.V., et al., *"HIFU Beam:" A Simulator for Predicting Axially Symmetric Nonlinear Acoustic Fields Generated by Focused Transducers in a Layered Medium.* IEEE Trans Ultrason Ferroelectr Freq Control, 2021. **68**(9): p. 2837-2852.
18. Gonzalez, R.C., R.E. Woods, and S.L. Eddins, *Digital Image processing using MATLAB*. 2004, Upper Saddle River, NJ: Pearson/Prentice Hall. xiv, 609 p.
19. Maxwell, A.D., et al., *Trapping of embolic particles in a vessel phantom by cavitation-enhanced acoustic streaming.* Phys Med Biol, 2014. **59**(17): p. 4927-43.
20. Rosnitskiy, P.B., et al., *Design of HIFU Transducers for Generating Specified Nonlinear Ultrasound Fields.* IEEE Trans Ultrason Ferroelectr Freq Control, 2017. **64**(2): p. 374-390.
21. O'Neil, H.T., *Theory of Focusing Radiators.* J. Acoust. Soc. Am. , 1949. **21**: p. 516–526.
22. Xu, Z., et al., *Effects of acoustic parameters on bubble cloud dynamics in ultrasound tissue erosion (histotripsy).* J Acoust Soc Am, 2007. **122**(1): p. 229-36.